NANO MICRO small

Supporting Information

for *Small,* DOI: 10.1002/smll.202204116

Electrochemical Generation of Catalytically Active Edge Sites in C_2N-Type Carbon Materials for Artificial Nitrogen Fixation

*Wuyong Zhang, Shaoqi Zhan, Qing Qin, Tobias Heil, Xiyu Liu, Jinyeon Hwang, Thimo H. Ferber, Jan P. Hofmann, and Martin Oschatz**

Supporting Information

Electrochemical Generation of Catalytically Active Edge Sites in C_2N-type Carbon Materials for Artificial Nitrogen Fixation

*Wuyong Zhang[+] Shaoqi Zhan,[+] Qing Qin[+] Tobias Heil, Xiyu Liu, Jinyeon Hwang, Thimo H. Ferber, Jan P. Hofmann, Martin Oschatz**

Experimental Details

Reagents and Synthesis:

Hexaketocyclohexane octahydrate, diaminomaleonitrile salicylic acid, sodium citrate, hydrochloric acid, para-(dimethylamino) benzaldehyde, acetic acid (AcOH, 99%), acetonitrile (MeCN, 99.8%) were purchased from Alfa Aesar. Standard NH_4^+-N solution (6 mg/L) was purchased from Merck. Unless otherwise stated, ultrapure (18.2 MΩ·cm) water was used in all experiments. All chemicals were used without further purification.

Synthesis of hexaazatriphenylene-hexacarbonitrile (HAT-CN): According to the procedure described in our previous report,[1] Hexaketocyclohexane octahydrate (4 g, 12.6 mmol) and diaminomaleonitrile (10.88 g, 100.8 mmol) were refluxed in AcOH (150 mL) for 2 h. The black suspension was filtered off while hot and washed with hot AcOH (3 × 25 mL) resulting in a black solid. The solid was suspended in 30 % HNO_3 (60 mL) and heated at 100 °C for 3 h. The hot dark brown suspension was poured into ice water (200 mL) and cooled overnight. The suspension was filtered and the solid was refluxed in MeCN (400 mL) for 2 h and was filtered. The filtrate was evaporated in vacuum to give an orange solid (2.4 g, yield 50 %).^{13}C NMR (DMSO-d^6, 100 MHz): δ 142.0, 135.8, 114.5.

Synthesis of HAT-Ts: According to the reported literature,[2] HAT-Ts were prepared using HAT-CN (200 mg) for carbonization in a horizontal tubular furnace at different temperatures (700 and 950 °C) for 1 h under Ar gas flow. The heating ramp was set to be 2 °C min^{-1}. The described resulting materials are labelled as HAT-Ts, where T represents the maximum synthesis temperature.

Characterization Methods:

High-resolution transmission electron microscopy (HRTEM) was performed on a JEOL ARM 200F microscope at an acceleration voltage of 200 kV. **Scanning electron microscopy** (SEM) was carried out on a LEO 1550-Gemini microscope operating at 3.00 kV. A platinum layer was sputtered on the samples to increase their surface conductivity. **Energy-dispersive X-ray** (EDX) investigations were conducted using a Link ISIS-300 system (Oxford Microanalysis Group) equipped with a Si(Li) detector and an energy resolution of 133 eV. **Powder X-ray diffraction** (PXRD) pattern were recorded on a Bruker D8 Advance diffractometer equipped with a scintillation counter detector with CuK_α radiation ($\lambda = 0.15184$ nm) applying a 2θ step size of 0.025°. **X-ray photoelectron spectroscopy** (XPS) data were obtained on a Physical Electronics PHI Versaprobe 5000 spectrometer in fixed analyzer transmission mode using monochromatic Al K_α radiation ($h\upsilon$ = 1486.6 eV, spot diameter 200 µm and a power of 50 W) at an angle of 45° with a pass energy of 23.50 eV (step size of 0.1 eV) for region scans. The samples have been measured on Indium foil and due to their good conductivity, no charge neutralization has been applied. Elemental compositions were determined using survey scans over a range of 1200–0 eV and a pass energy of 187.85 eV using Scofield relative sensitivity factors available in CasaXPS version 2.3.23. **EPR studies** were conducted on Bruker EMXnano benchtop X-Band EPR spectrometer. Samples of HAT-700-A were scraped from the electrode and filled into an EPR cell under within an Argon-filled glovebox. **C/H/N Elemental analysis** (EA) was accomplished as combustion analysis with a Vario Micro device. **N_2 physisorption measurements** were performed on a Quantachrome Autosorb IQ apparatus with sample weight of ~50 mg. Before each test, the samples were degassed under vacuum at 140 °C for overnight. The pore size distributions were calculated using quenched solid density

functional theory (QSDFT) method (adsorption branch kernel). The specific surface areas (SSAs) were calculated using the multi-point Brunauer-Emmett-Teller (BET) model (p p_0 determined at p/p_0 = 0.005–0.05). For the measurements of CO_2 physisorption of the electrodes before and after electrochemical activation on a Quantachrome Quadrasorb apparatus at 273 K, two electrodes with similar mass loading were prepared. One of them went through electrochemical activation first and was then degassed under vacuum at 80 ^oC overnight.

Electrochemical Measurements:

All electrochemical measurements were operated at room temperature in a three-electrode system on an Autolab potentiostat (Metrohm). A carbon paper (1×1 cm^2) was selected as the working electrode support, the Pt electrode (1×1 cm^2) and saturated calomel electrode (SCE) severed as the counter and reference electrode, respectively. All potentials in this work are referred to RHE via the correction (0.059*pH+0.242) V. The experiments were conducted in a H-cell with a 40 mL volume for each side separated by a Nafion 117 membrane, which was pre-treated by boiling in 5% H_2O_2 solution for 1 h at 80 ^oC, rinsing in DI water, boiling in DI water for 1 hr and then in 0.5 M H_2SO_4 solution for 1 hr at 80 ^oC, and then rinsing in DI water again. Before the catalytic tests, 1 mg catalyst was dispersed in 100 μL ethanol and 20 μL Nafion solution (5 wt%) and sonicated for 30 min to get a homogenous catalyst ink. The catalyst ink was then drop cast onto carbon paper to get the working electrode and dried it in the oven at 80 ^oC for 4 h. Before each test, the electrolyte was purged with argon or nitrogen for 30 min with a flow rate of 30 mL/min. A gas flow rate of ~10 mL/min has been applied during the LSV and CV tests. All the gases in this work have been passed through solid $Ca(OH)_2$ and $CaCl_2$ prior to their supply to the reaction solution to remove possible impurities. All the reported results have been obtained with nitrogen gas from a central gas supply based

on a liquid nitrogen tank. In order to verify the results obtained, high-purity (99.999%) nitrogen (Linde) has been used in control experiments in a different laboratory. For the control measurements with the nitrogen (5.0) gas from the gas bottle, an updated gas scrubbing protocol with 0.5 M $KMnO_4$ and 0.5 M KOH solutions has been applied.

CV was used to activate HAT-700 under Ar atmosphere with a scan rate of 100 mV/s, the mark of activation complete is the stable CV, for mass loading of 1 mg cm^{-2}, the cycle numbers were set to 2000, otherwise, galvanostatic method with the current density of -10 mA cm^{-2} on working electrode for 8 h is also available. After CV activation procedure, electrochemical performance of as-prepared materials was examined by LSV first with the scan rate of 1 mV/s under different atmosphere. All electrolysis operations were conducted under continuous gas feed, FE of the ammonia was calculated from the percentage of the total amount of the charge produced by ammonia (n_{NH_3}) in the total charge Q (C) passed through the electrochemical system. Since three electrons are transferred for the formation of one ammonia molecule, the FE can be calculated as follows: $FE= n_{NH_3} \times 3F/ (I \times t)$, where the F is the Faraday constant (96485.34 C/mol), I (A) is the current at the potential applied on the electrochemical system, t (s) is the electrolysis time. Three parallel chronoamperometry experiments have been conducted under similar conditions to check for reproducibility of the results and to make statistical analysis possible. ^{1}H NMR spectra of ^{15}N isotope labelling experiment were tested for the post-electrolysis 0.1 M HCl electrolyte with feeding gas of $^{14}N_2$, $^{15}N_2$, respectively. The gas purity of the used $^{15}N_2$ (purchased from Sigma Aldrich) is given with 99% with 98 atom% of $^{15}N_2$. Because of the high price of $^{15}N_2$, the gas flow was set to be slowly bubbling for saving gas. To increase the concentration of NH_4^+ in electrolyte to detectable levels, before NMR test, the electrolyte in cathode (40 mL) was

concentrated to 1 mL by evaporating excessive water in an 80 ^{o}C water bath, and the final pH of the electrolyte for NMR was adjusted to be 1.

Detection of NRR Products:

The concentrations of ammonium and hydrazine in the electrolyte were analyzed with the indophenol blue method and the Watt-Chrisp method,[3] respectively. For ammonium, 2 mL electrolyte was mixed with 2 mL chromogenic reagent of 1 M NaOH solution (containing 5 wt% of salicylic acid and 5 wt% of sodium citrate), followed by adding 1 mL oxidizing solution of 0.05 M NaClO solution and 0.2 mL of 1 wt% sodium nitroferricyanide as catalyzing reagent. After standing at room temperature for 1 h, the produced indophenol blue was detected by UV-Vis spectroscopy. The standard curve was plotted with the absence value at 655.5 nm and the concentration of standard NH_4^+ solution.

For hydrazine, 2 mL of electrolyte was mixed with 2 mL of the chromogenic reagent which collected with concentrated hydrochloric acid (3 mL), anhydrous ethanol (30 mL) and para-(dimethylamino) benzaldehyde (599 mg), after stirring at room temperature for 10 min, the absorption spectrum of solution was also measured on UV-Vis but the characteristic peak was changed to 455 nm which confirm the formation of hydrazine.

For the test for nitrate and nitrite contaminations in the electrolyte, nitrogen gas was supplied to the electrolyte solution at a flow rate of 30 mL/min over night. For nitrate detection,[4] 0.1 mL 1 M HCl and 0.01 mL 0.8 wt% sulfamic acid solution were added to 5 mL of the electrolyte after gas supply. The absorption spectrum was tested using an ultraviolet-visible spectrophotometer and the absorption intensities at wavelengths of 220 and 275 nm were recorded. The final absorbance value was calculated using the equation: $A=A_{220nm}-2A_{275nm}$.The concentration-absorbance calibration curve was recorded using a series of standard NO_3^--N solutions.

For nitrite detection,[5] firstly, 0.2 g of N-(1-naphthyl) ethylenediamine dihydrochloride, 4 g of p-aminobenzenesulfonamide, and 10 mL of phosphoric acid ($\rho = 1.685$ g mL^{-1}) were added into 50 mL of deionized water and mixed thoroughly as the color reagent. When testing the electrolyte from electrolytic cell, it should be diluted to the detection range. Then 5 mL of the diluted electrolyte and 0.1 mL of color reagent were mixed. After 20 min at room temperature, the UV-Vis absorption spectrum was measured and the absorption intensity was recorded at a wavelength of 540 nm. The concentration-absorbance calibration curve was recorded using a series of standard NO_2^--N solutions.

Computational Section:

All the DFT calculations were performed by the Vienna ab initio simulation package (VASP).[6] The electron-core interactions were described by the projected augmented wave (PAW)[7] method and electron exchange–correlation was expressed at the general gradient-approximation (GGA) level by the Perdew–Burke–Ernzerhof (PBE) functional.[8] A cutoff energy of 500 eV was adopted for the plane-wave basis set. All calculations were performed with spin polarization. For structural optimization, a convergence threshold of 0.03 eV $Å^{-1}$ was set in force and the total energy converged to within 10^{-5} eV. To better evaluate the van der Waals' interaction, Grimme's method (DFT-D3)[9] was included during the surface adsorption. The Gamma-point was considered for sampling the Brillouin zone during the calculations. A vacuum layer of at least 10 Å was used above the slab to avoid periodic interactions. The standard hydrogen electrode (SHE) model proposed by Nørskov,[10] in which the chemical potential of a proton-coupled-electron pair is equal to half of the chemical potential of H_2, was used to calculate the Gibbs free energy (ΔG). Therefore, the ΔG of all nitrogen reduction reactions (NRR) were computed by $\Delta G = \Delta E + \Delta ZPE - T\Delta S$, where ΔE is the electronic energy difference,

ΔZPE is the change of zero-point energy, and ΔS is the change of the entropy. The ZPE and entropies S were calculated by the vibrational frequencies of all species in which only vibrational mode of the adsorbed species are computed explicitly and the surfaces are fixed.

Supplementary Figures

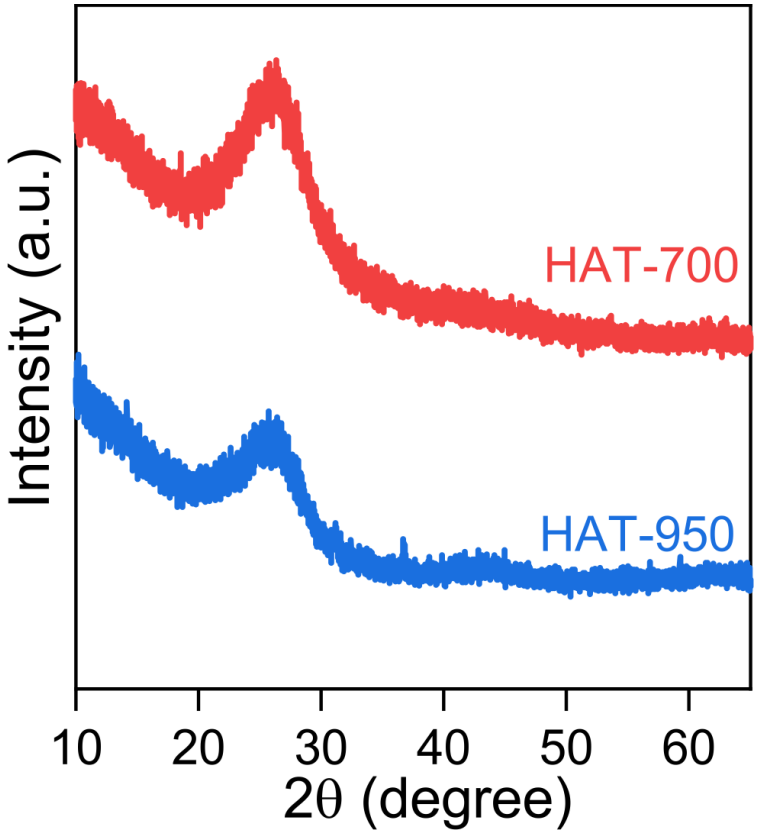

Figure S1. XRD patterns of HAT-700 and HAT-950.

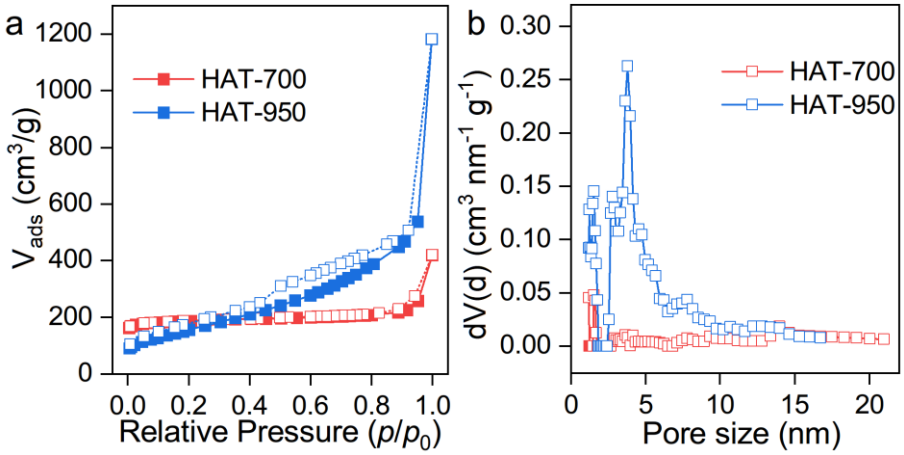

Figure S2. (a) N_2 physisorption isotherms (at -196 °C) of HAT-700 and HAT-950 with the corresponding (b) differential pore size distribution plots calculated with QSDFT.

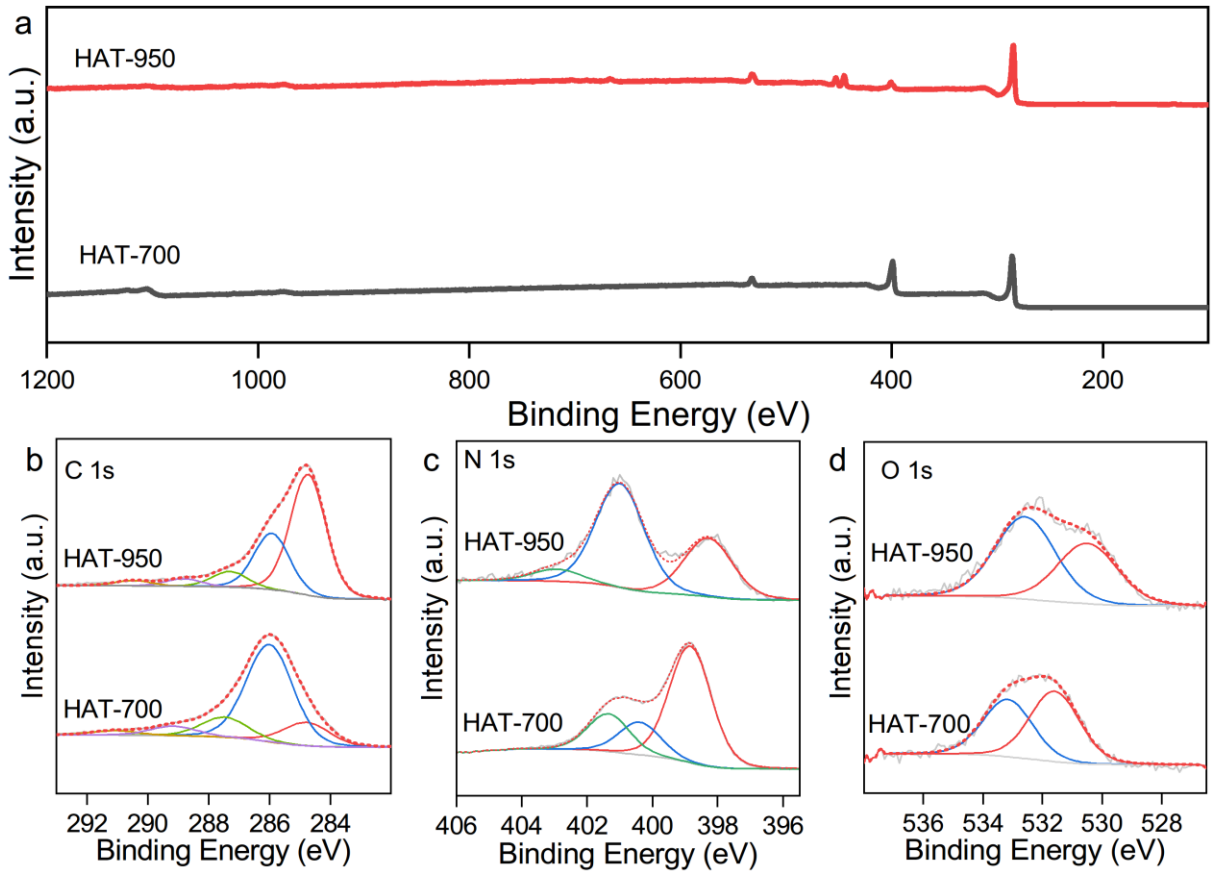

Figure S3. (a) XPS survey spectra of HAT-Ts and (b) corresponding deconvoluted C 1s, (c) N 1s and (d) O 1s spectra.

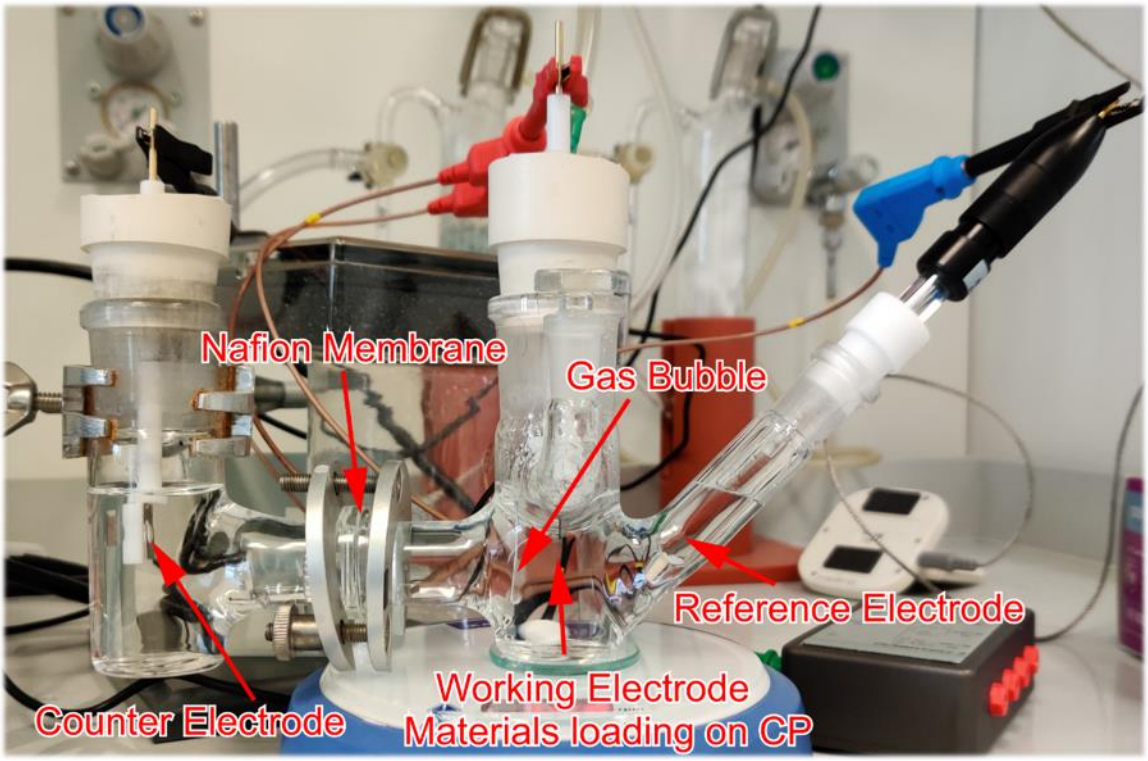

Figure S4. The digital picture of the H-cell setup for electrochemical NRR.

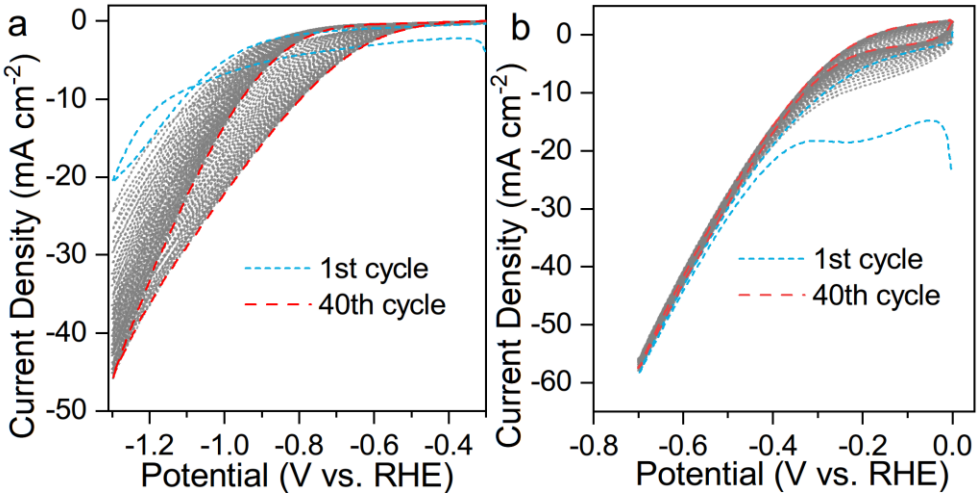

Figure S5. CV curves of 40 cycles of (a) HAT-700 and (b) HAT-950.

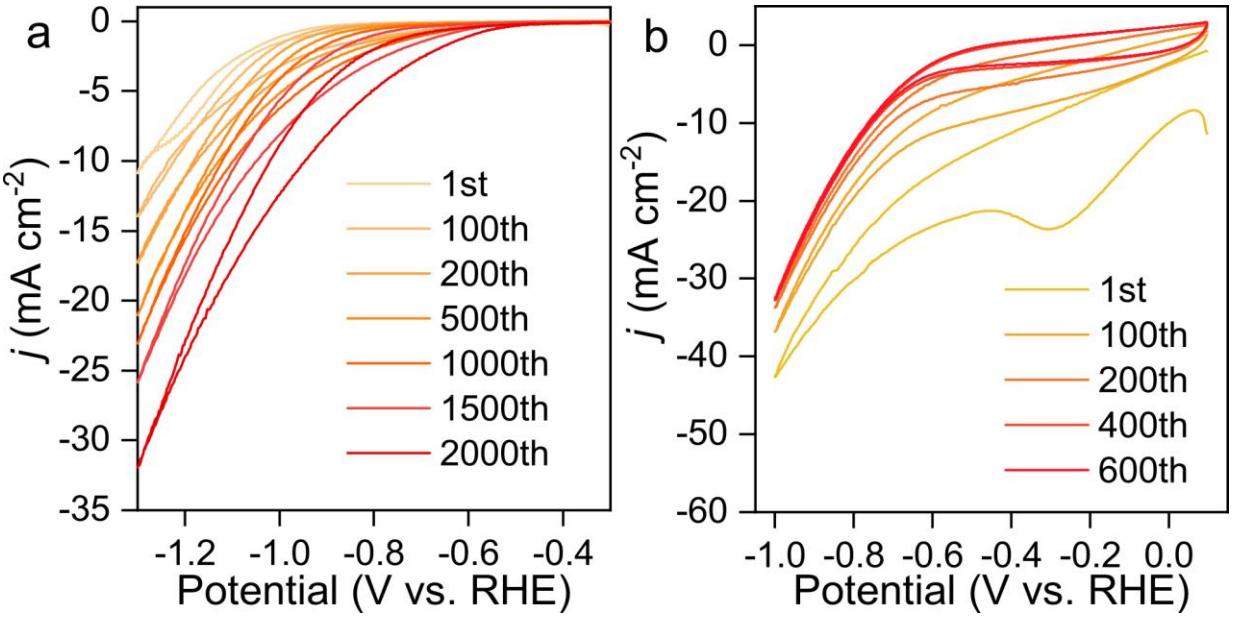

Figure S6. CV etching process of (a) HAT-700 and (b) HAT-950 at a rate of 100 mV/s.

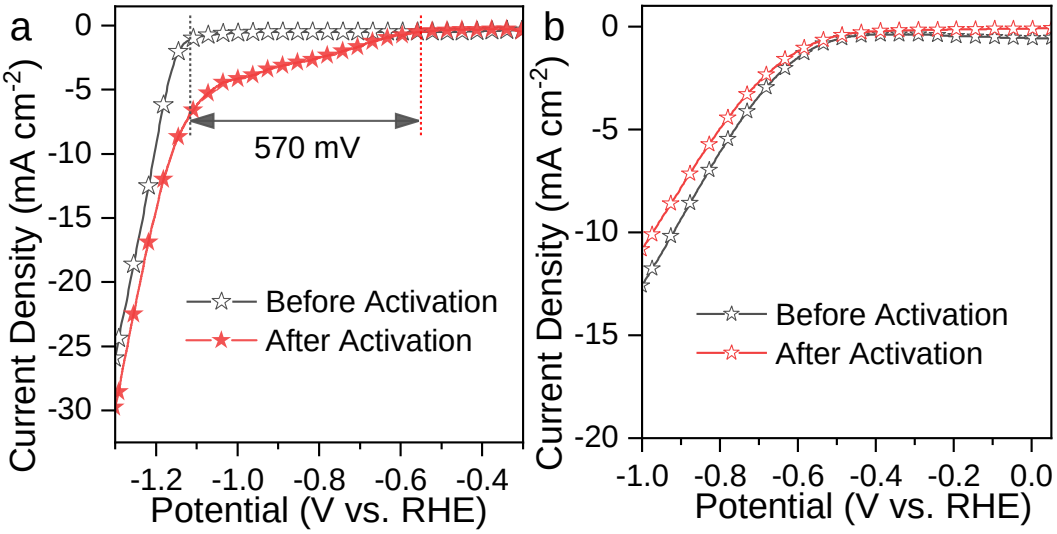

Figure S7. LSV curves of (a) HAT-700 and (b) HAT-950 in nitrogen-saturated electrolyte before and after 2000 cycles CV etching.

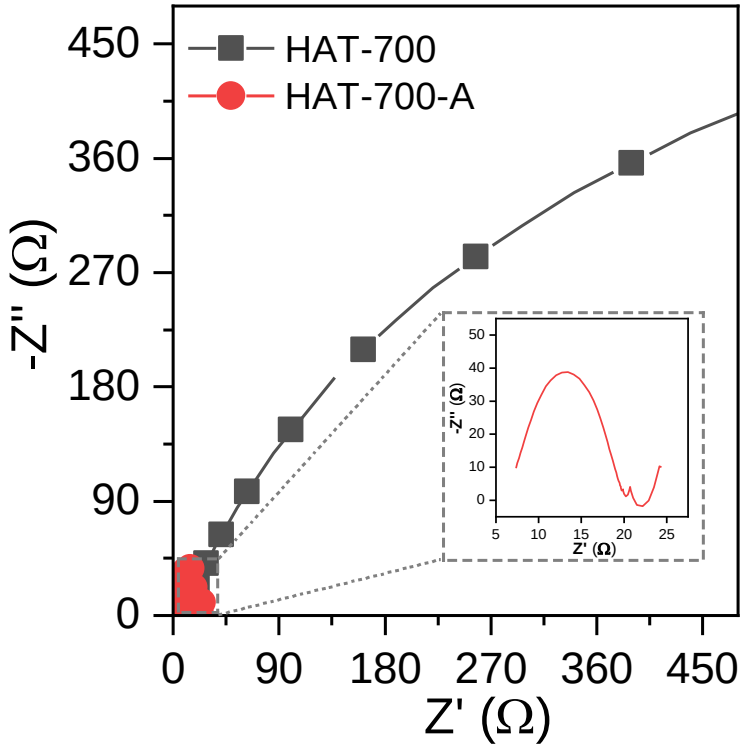

Figure S8. Electrochemical impedance spectroscopy (EIS) curves of HAT-700 and HAT-700-A.

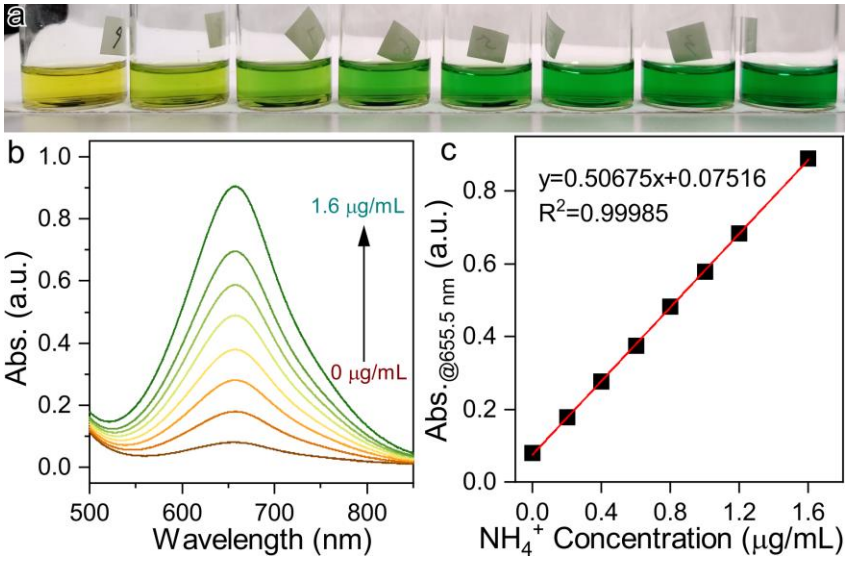

Figure S9. (a) Digital photo of different ammonia concentration with indophenol blue method coloration, (b) the corresponding UV-Vis spectroscopy curves and the absorbance at 655.5 nm was referred to the concentration of NH_4^+ and (c) corresponding calibration curve used for NH_4^+ calculation.

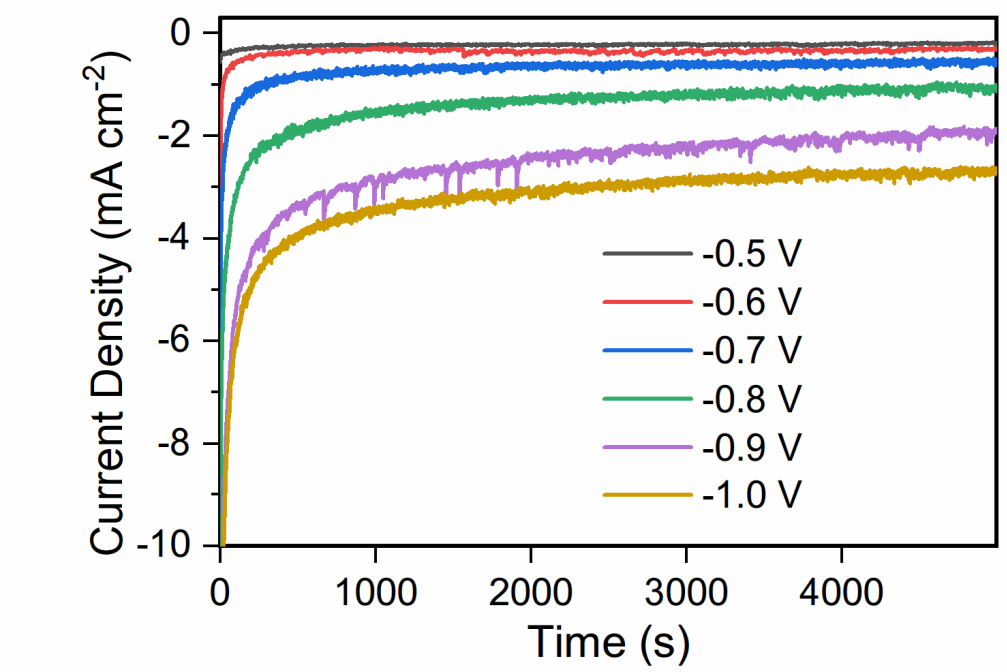

Figure S10. Chronoamperometry results of HAT-700-A at all given potentials.

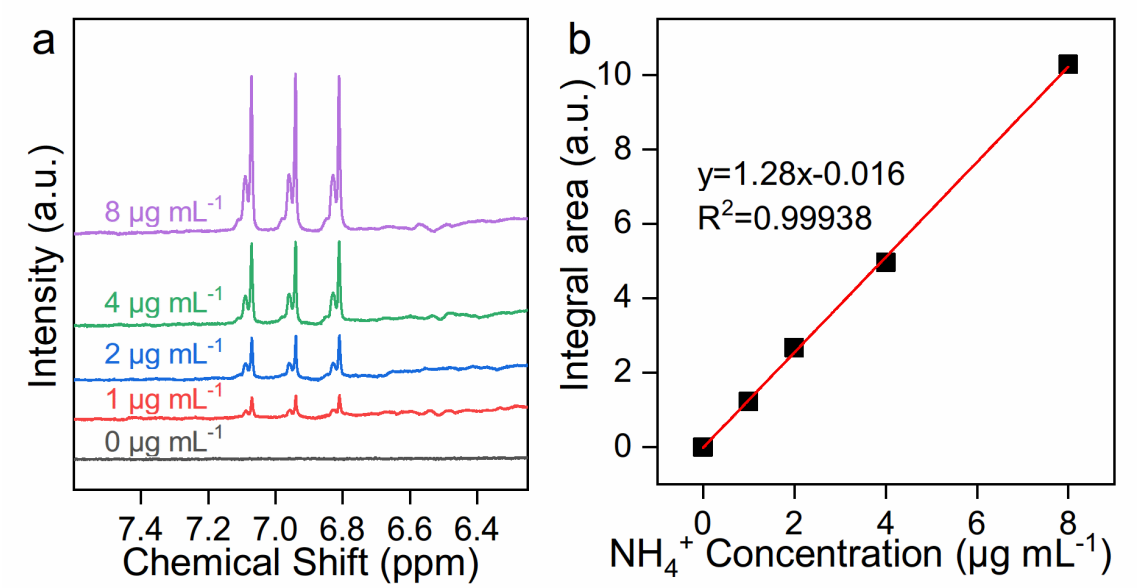

Figure S11. (a) ^{1}H NMR spectrum of NH_4^+ with different concentrations and (b) corresponding standard curve.

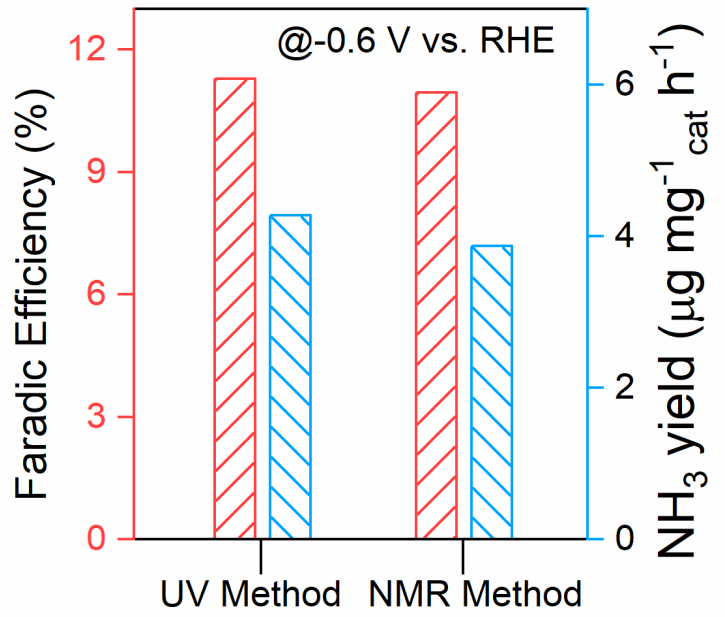

Figure S12. FE and NH_3 yield comparison between different methods.

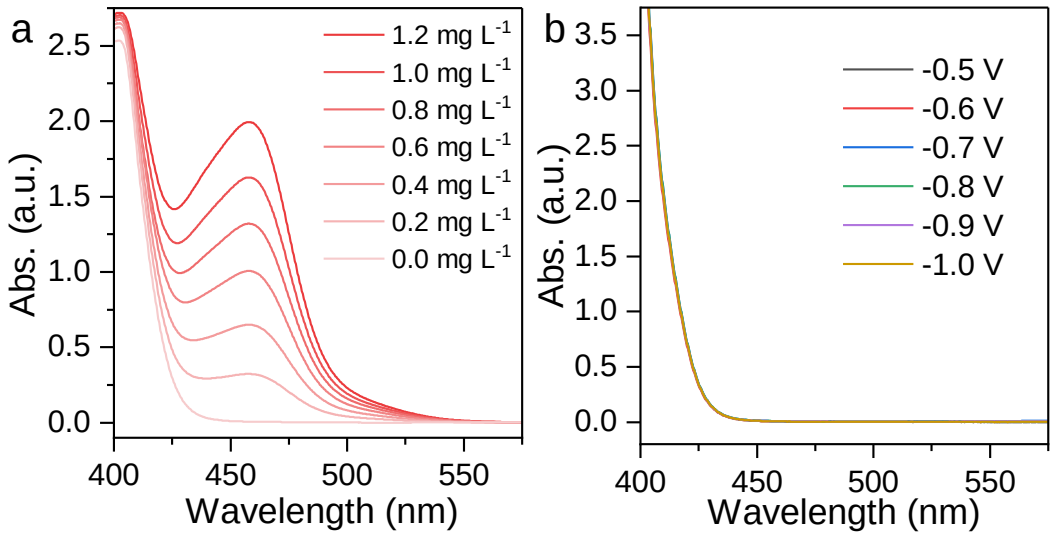

Figure S13. (a) UV-Vis spectra of N_2H_4 with different concentrations. (b) UV-Vis spectrum of electrolyte for possible hydrazine detection.

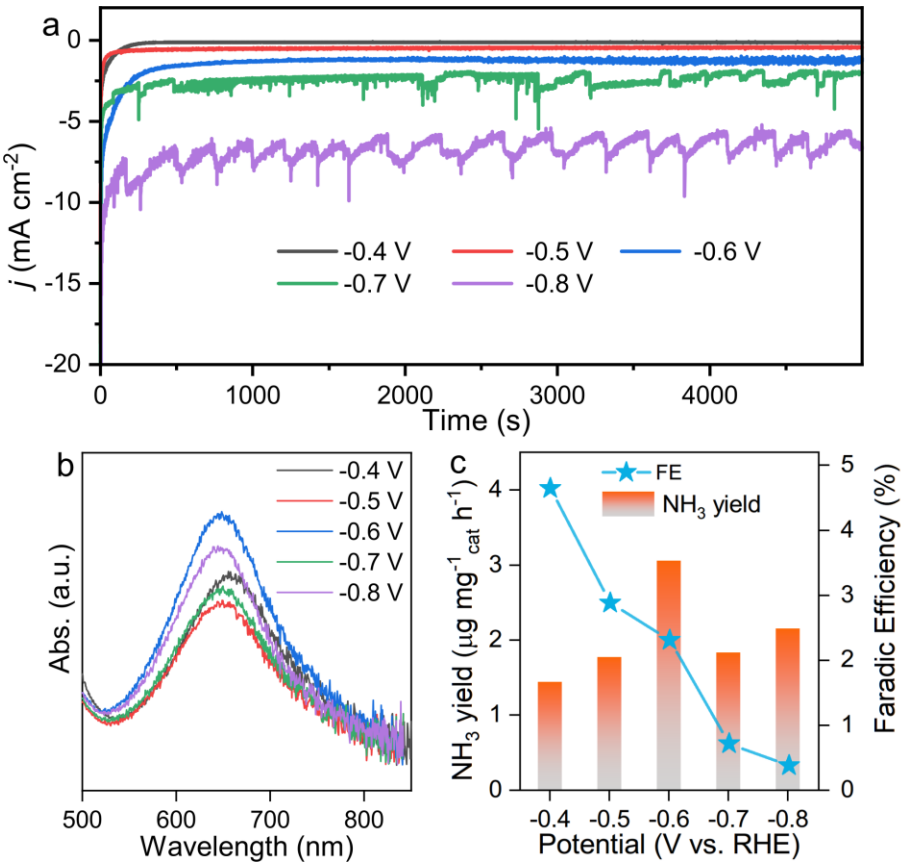

Figure S14. (a) Chronoamperometry results, (b) electrolyte UV-Vis spectra and (c) FE, NH_3 yield of HAT-950 at all given potentials.

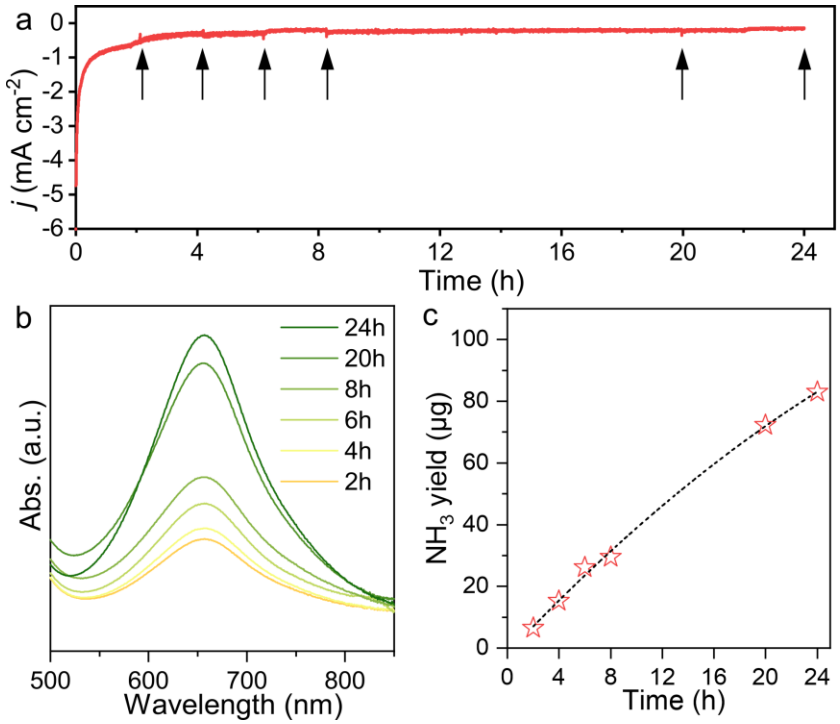

Figure S15. (a) Long-term chronoamperometry result of HAT-700-A, (b) UV-Vis tracking spectrum and (c) NH_3 yield tracking during 24-h test.

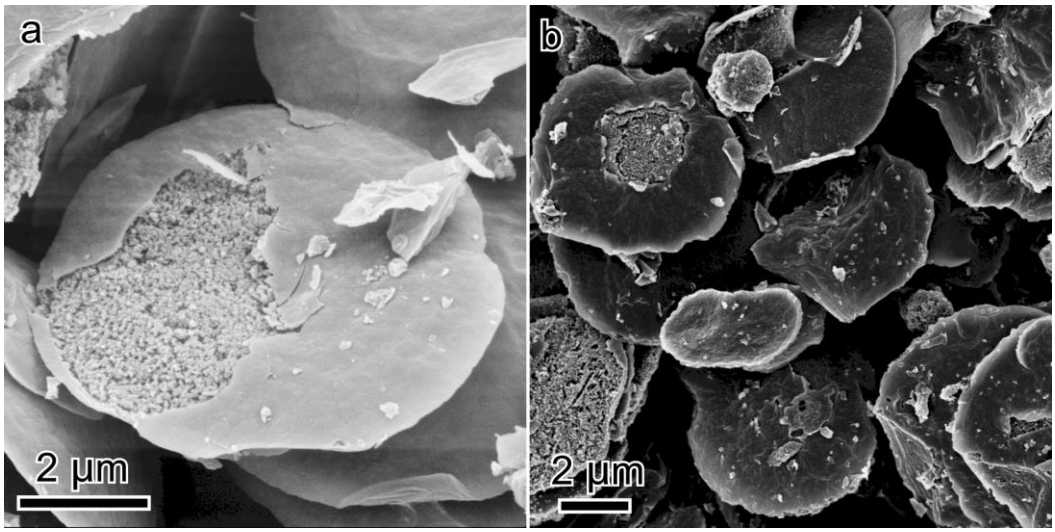

Figure S16. SEM images of HAT-700 (a) before and (b) after 24 h electrolysis.

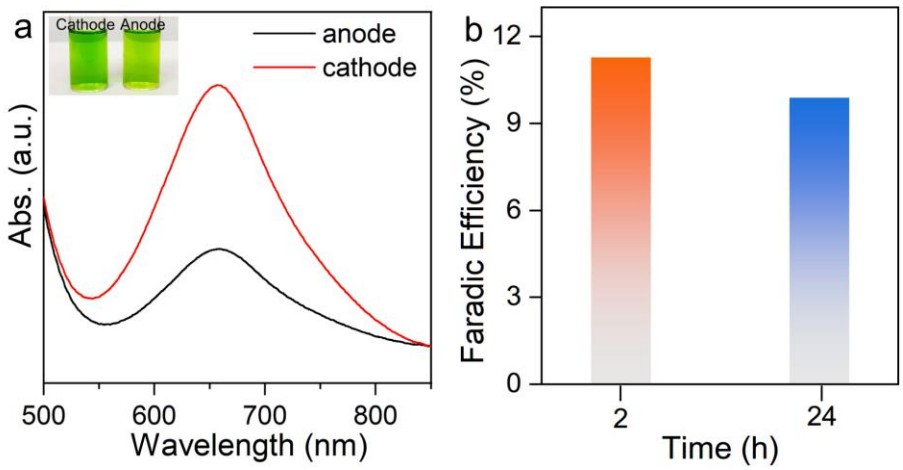

Figure S17. (a) UV-Vis spectrum of electrolyte collected after 24 h electrolysis and (b) The FE comparison between 2 h and 24 h calculated in the cathodic and anodic electrolyte.

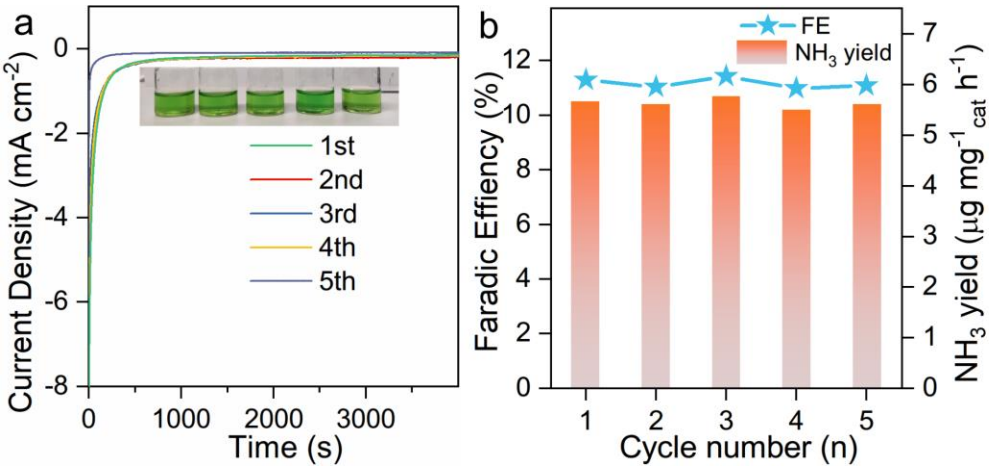

Figure S18. (a) Chronoamperometry results and (b) corresponding FE and NH_3 yield of the five consecutive NRR cycles.

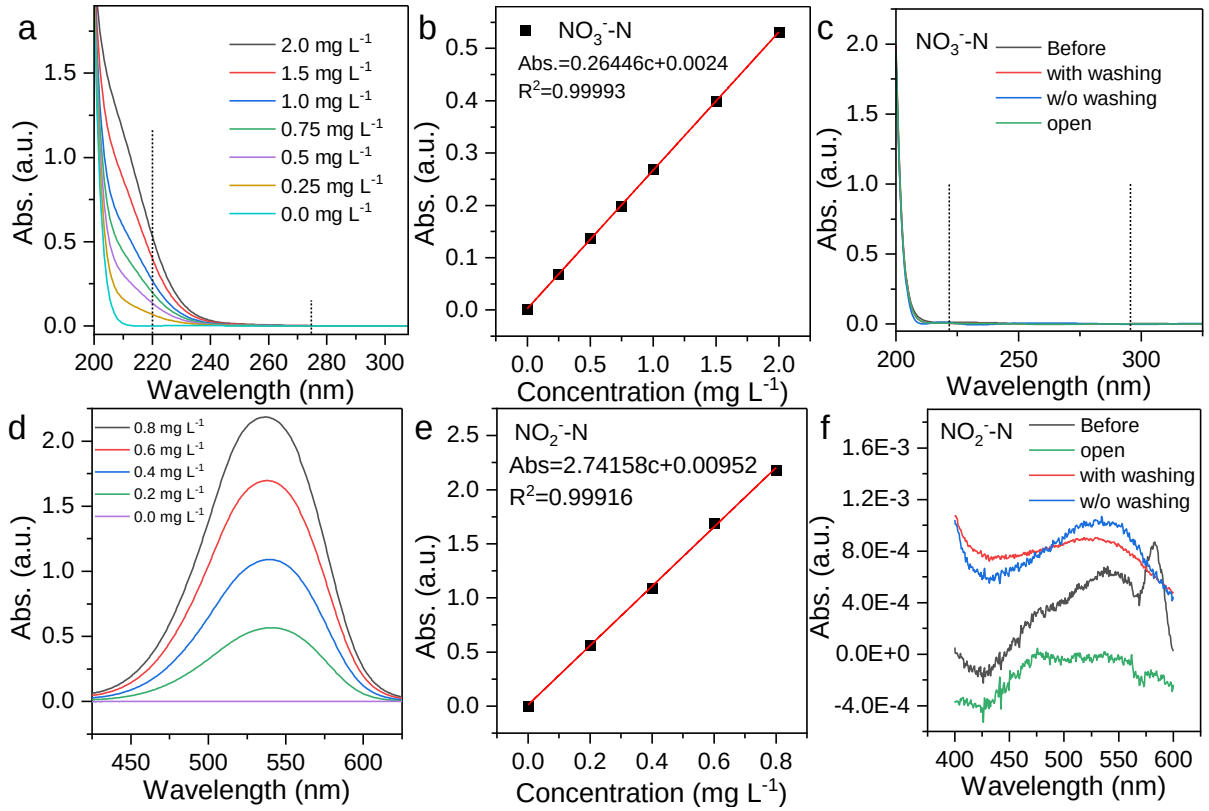

Figure S19. Nitrate and nitrite detection in the reaction solutions. (a-c) UV-Vis spectra, calibration curve with different nitrate concentration and UV-Vis spectra of the electrolyte under different conditions. (d-f) UV-Vis spectra, calibration curve with different nitrite concentration and UV-Vis spectra of the electrolyte under different conditions.

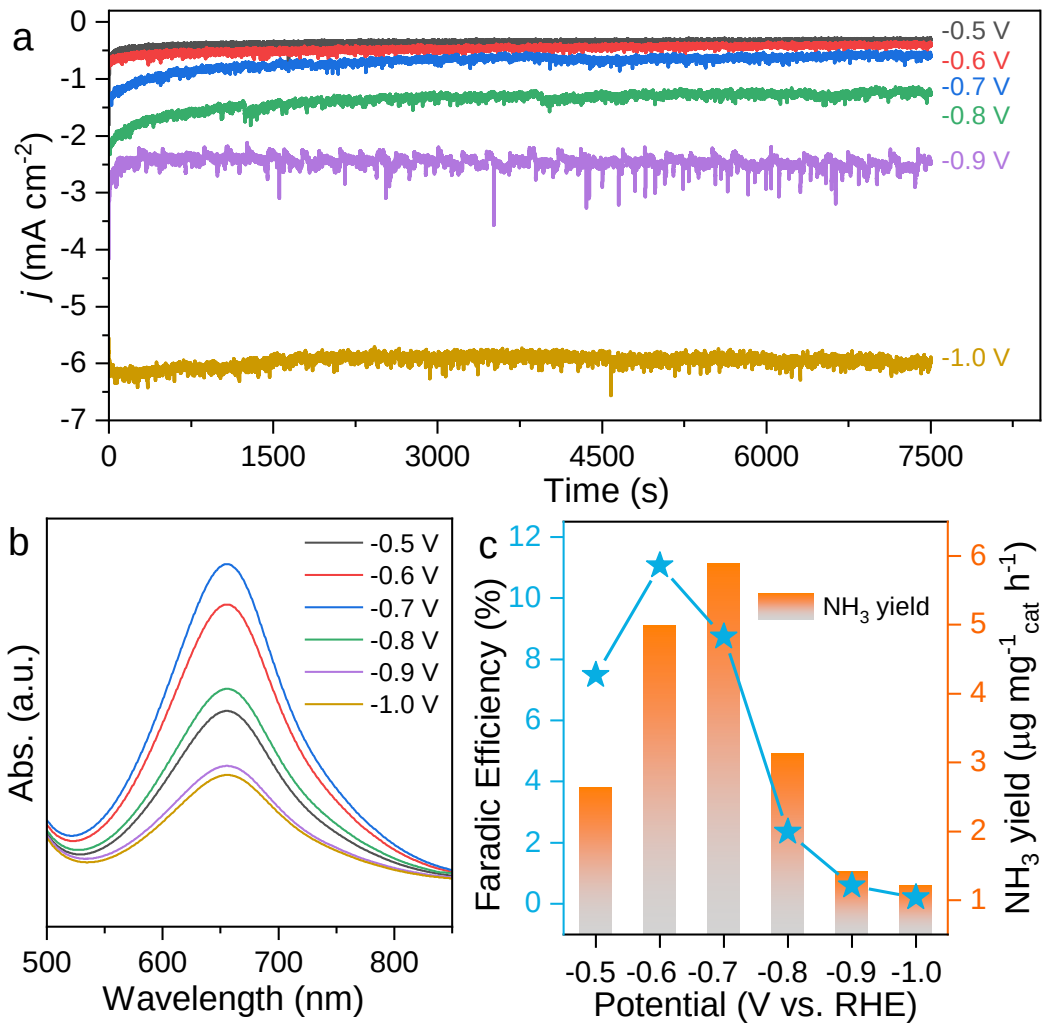

Figure S20. Control experiment of the NRR properties of HAT-700-A obtained with nitrogen of 99.999% purity. (a) Chronoamperometry results, (b) UV-Vis spectra of electrolytes colored with the indophenol blue method and (c) FE, NH_3 yield at all given potentials.

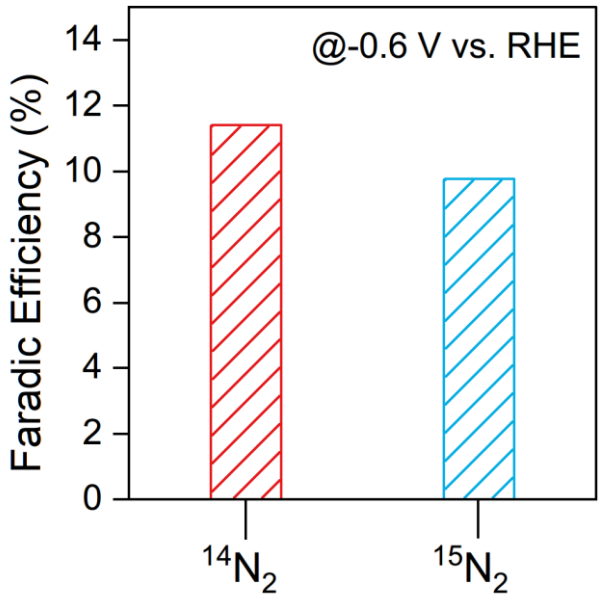

Figure S21. Comparison of the FE obtained with $^{14}N_2$ and $^{15}N_2$ as feeding gas at -0.6 V vs. RHE.

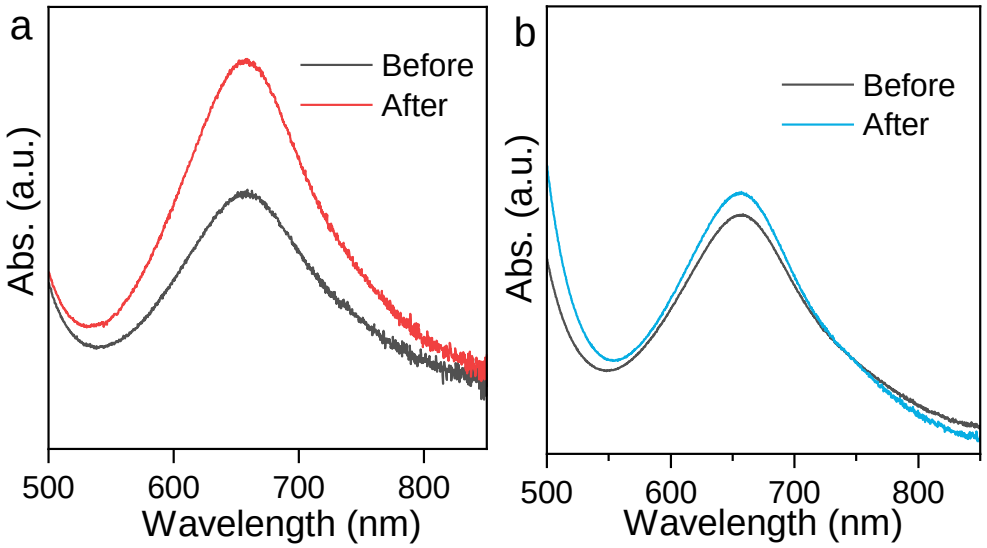

Figure S22. UV-Vis spectrum changes of 0.1 M HCl with (a) HAT-700 and (b) HAT-950 as working electrode after 2000 CV cycles etching with indophenol blue method.

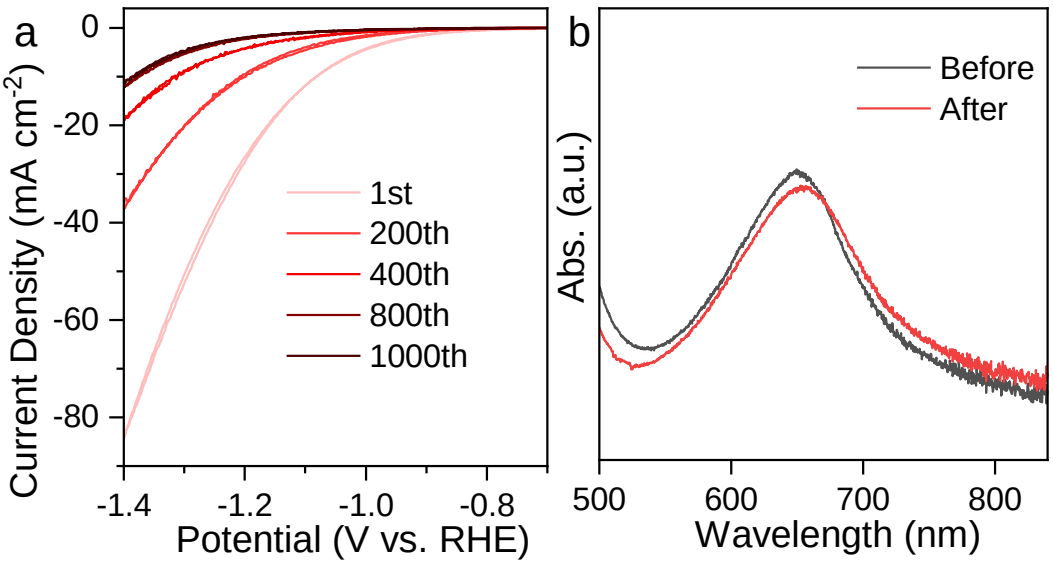

Figure S23. (a) CV curves of HAT-700 with 1000 cycles in 0.1 M PBS electrolyte and the UV-Vis spectrum change of the electrolyte before and after CV etching.

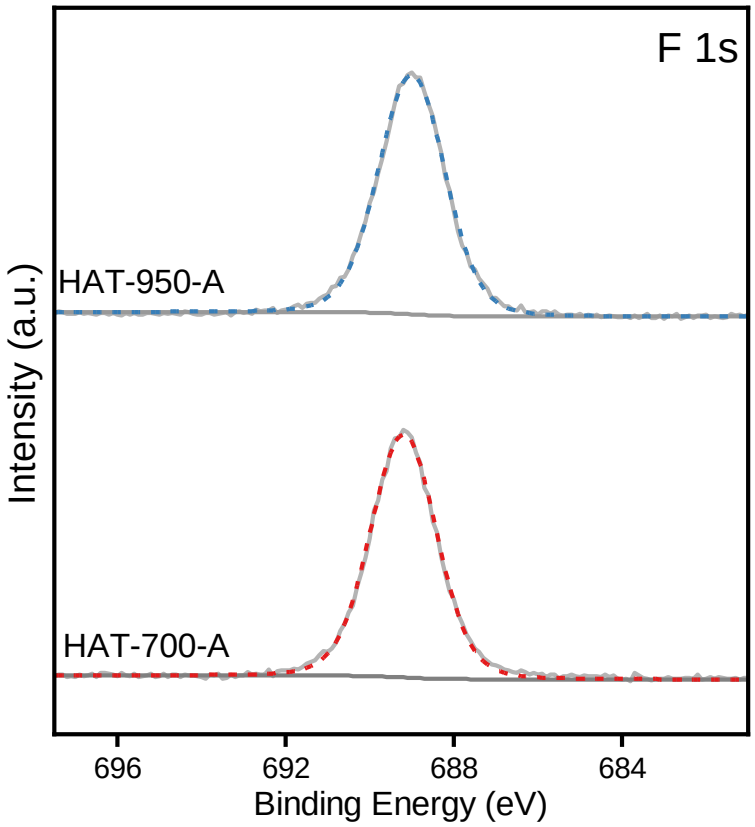

Figure S24. High resolution F 1s XPS spectrum of HAT-Ts after CV etching.

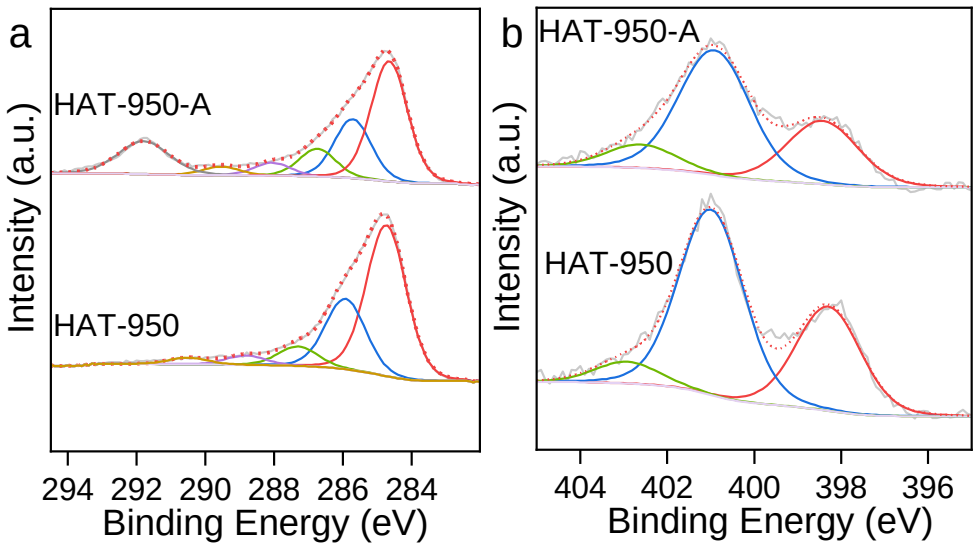

Figure S25. (a) Deconvoluted C 1s XPS spectra and (b) N 1s XPS spectra of HAT-950 and HAT-950-A.

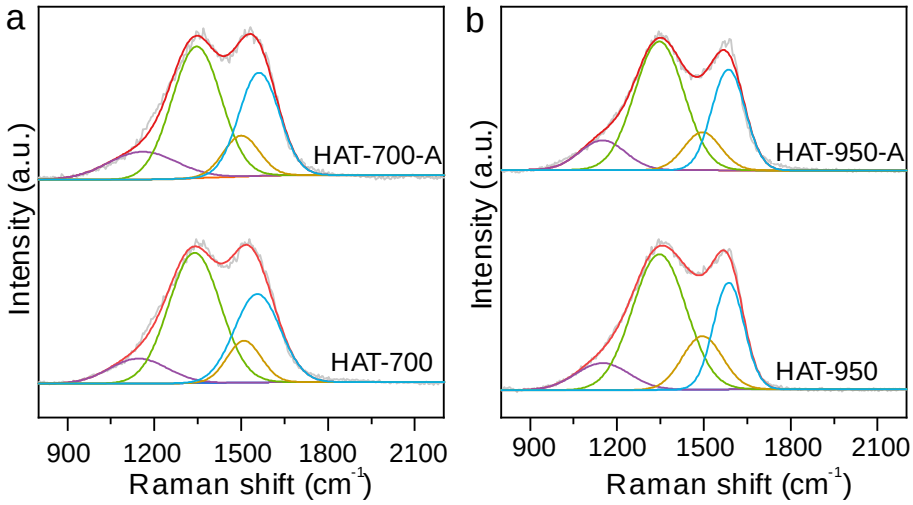

Figure S26. Raman spectra of (a) HAT-700 and (b) HAT-950 before and after electrochemical etching.

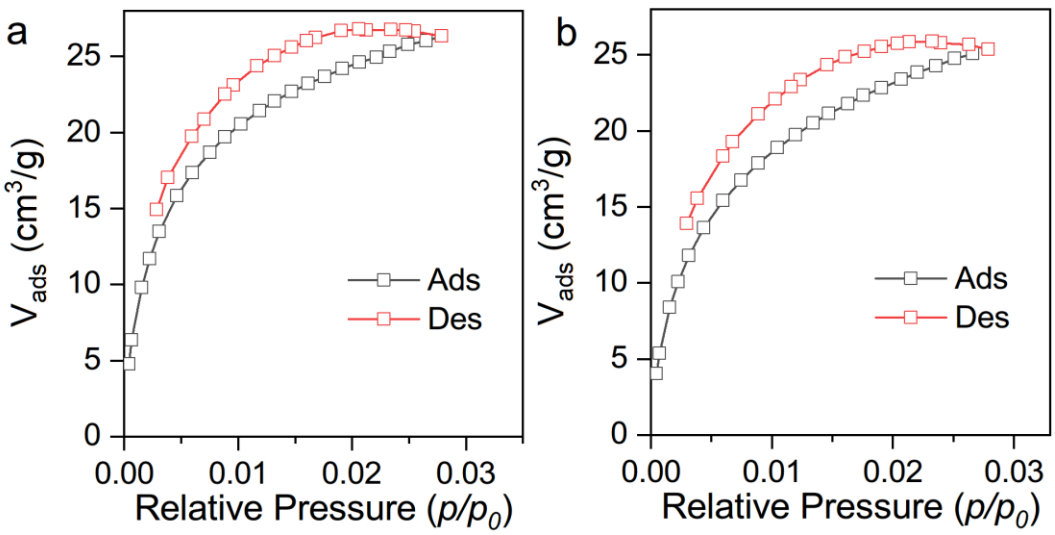

Figure S27. CO_2 physisorption isotherms of HAT-700 (a) and HAT-700-A (b) at 273 K.

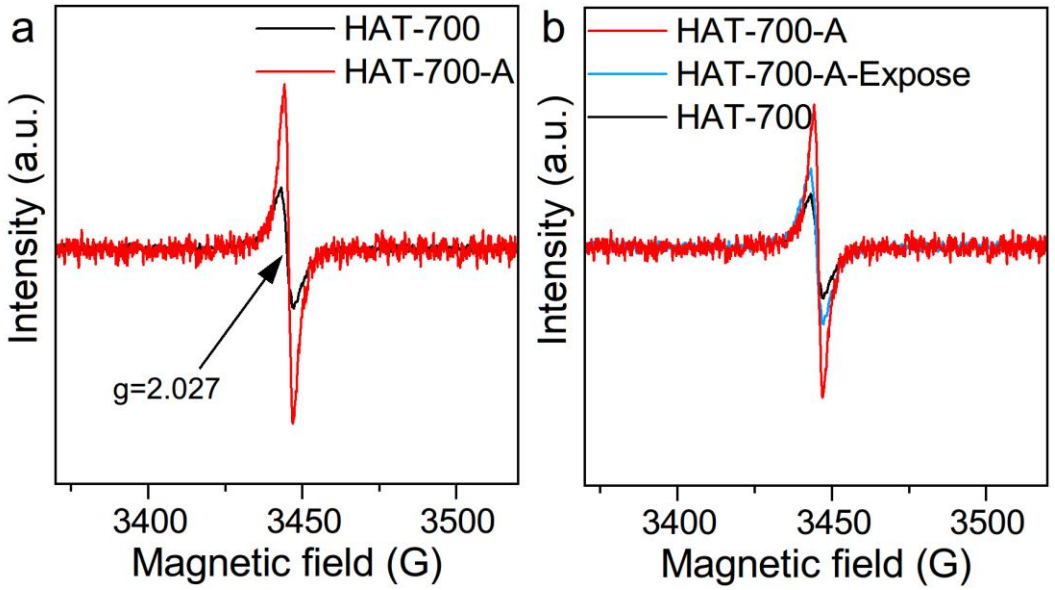

Figure S28. (a) Electron paramagnetic resonance (EPR) spectra of HAT-700 before and after electrochemical activation. (b) Additional EPR spectrum of HAT-700-A after exposure to air.

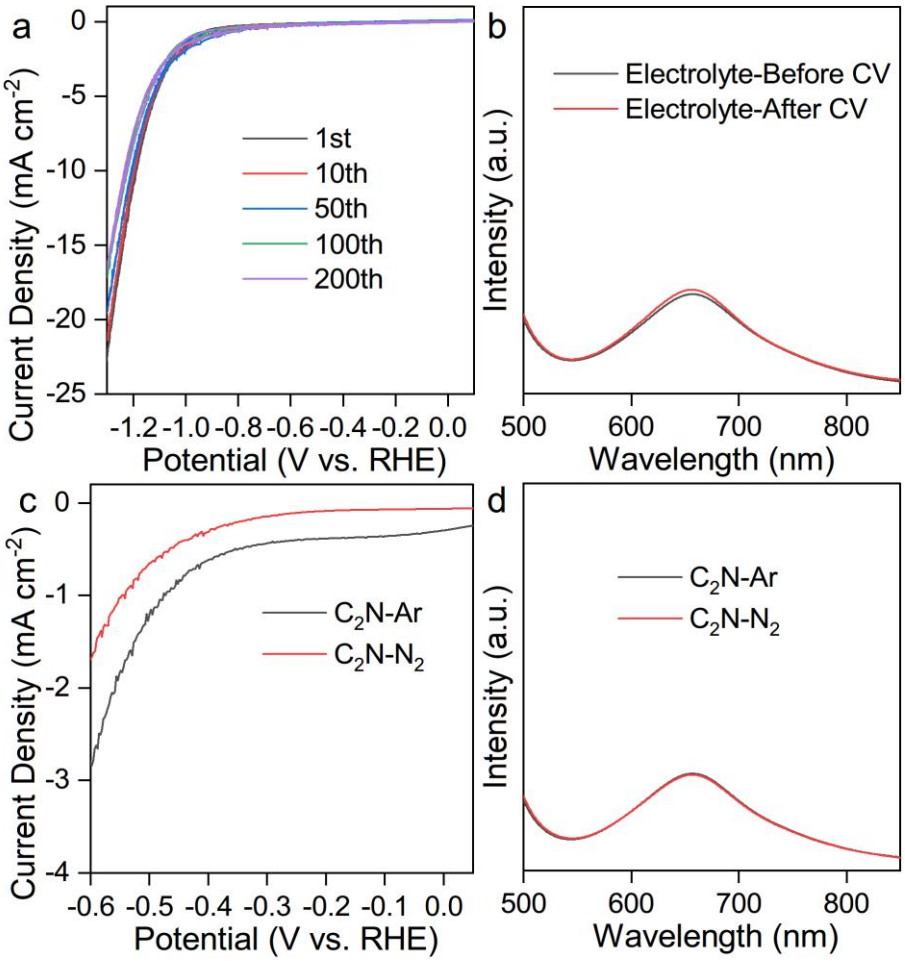

Figure S29. Electrochemical performance of C_2N without terminal nitrile groups. (a) CV curves of 200 cycles, (b) UV-Vis spectrum of the electrolyte before and after CV colored by the indophenol blue method, (c) LSV curves of C_2N under Ar and N_2 atmosphere, and (d) UV-Vis spectrum of electrolyte after electrolysis with C_2N under different atmospheres.

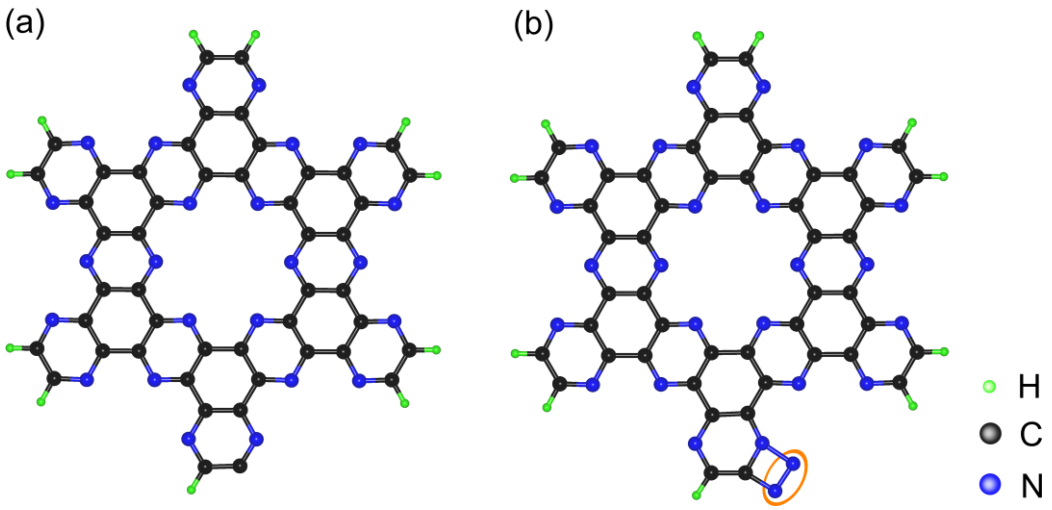

Figure S30. The optimized structure of the model (a) and side-on adsorption of N_2 molecule (b) The adsorbed N_2 has been marked with brown circle.

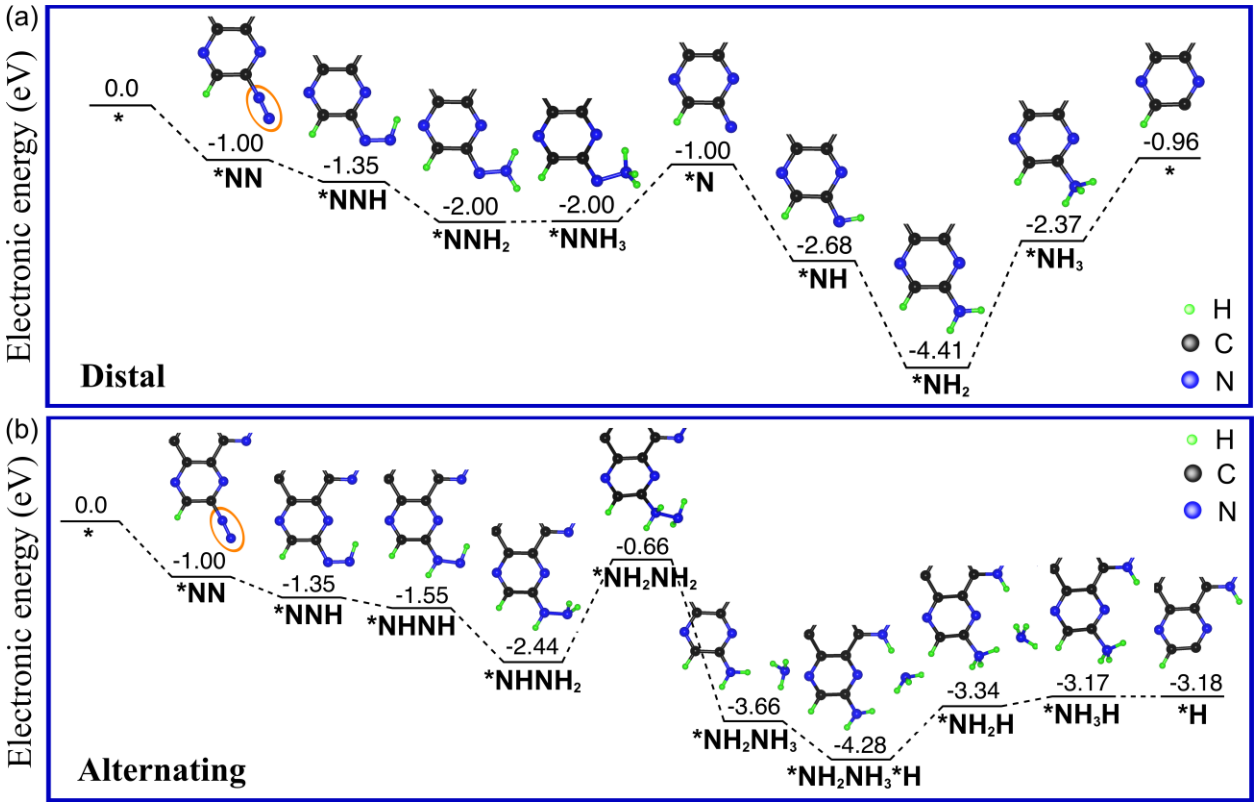

Figure S31. The energy panels of the distal (a) and alternating (b) pathways through end-on adsorption of N_2 on the sp^2-C. The adsorbed N_2 has been marked with brown circle.

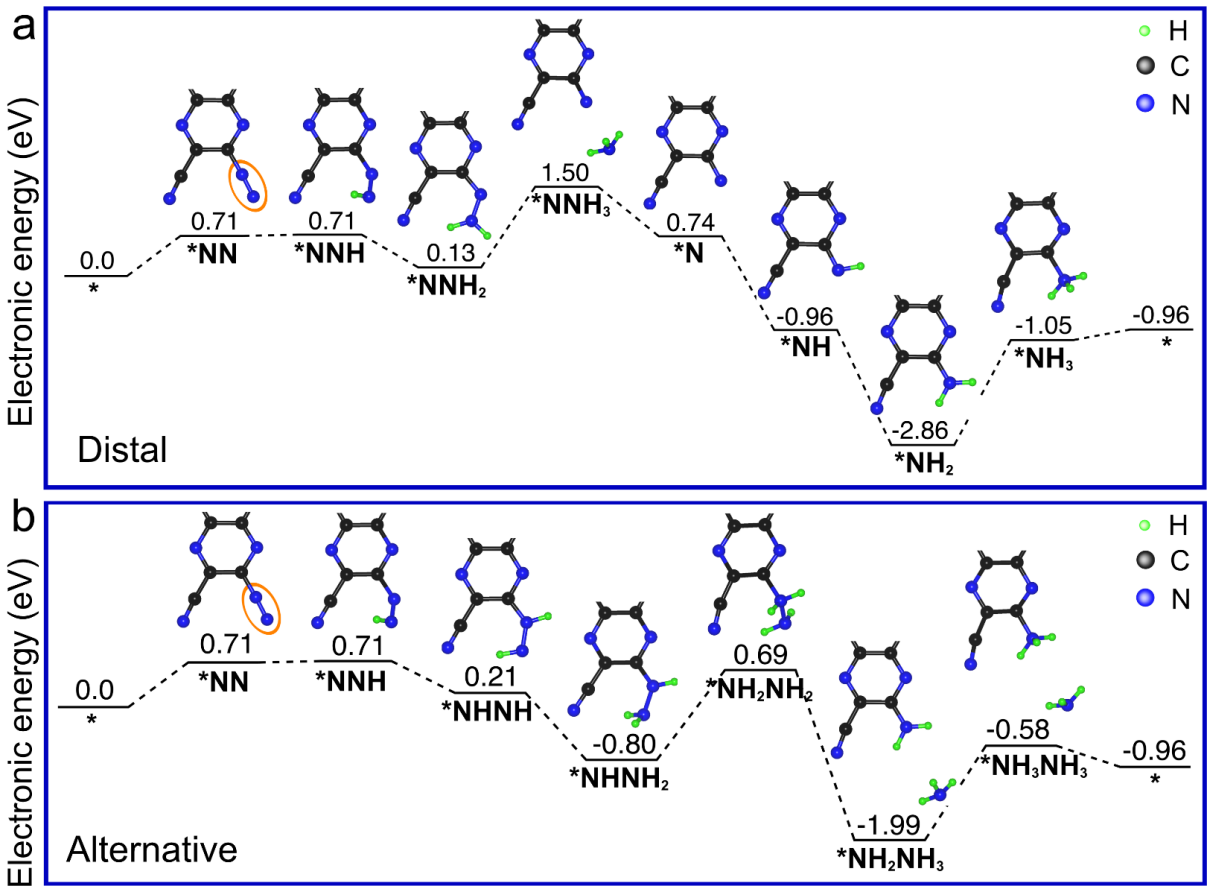

Figure S32. The energy panels of the distal (a) and alternative (b) pathways via the end-on adsorption of N_2 molecule, for the model of the neighboring carbon of the sp^2-C bonded with -CN group. On this model, the side-on adsorption of N_2 molecule has a very high adsorption free energy of 2.51 eV, which is unfavorable to react via this pathway. The adsorbed N_2 has been marked with a brown circle.

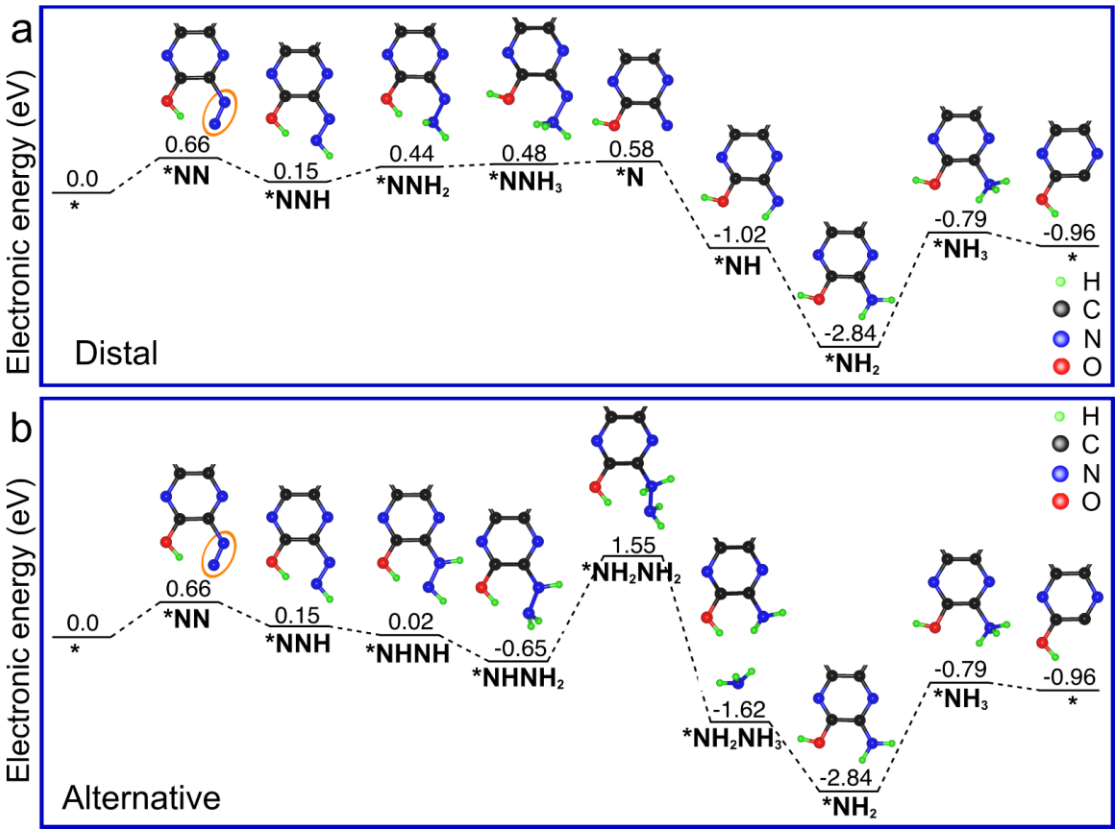

Figure S33. The energy panels of the distal (a) and alternative (b) pathways via the end-on adsorption of N_2 molecule, for the model of the neighboring carbon of the sp^2-C bonded with -OH group. On this model, the side-on adsorption of N_2 molecule has a very high adsorption free energy of 2.59 eV, which is unfavorable to react via this pathway. The adsorbed N_2 has been marked with a brown circle.

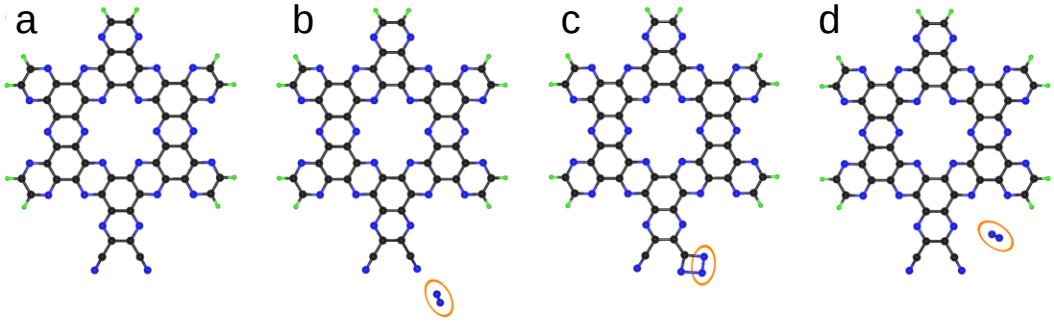

Figure S34. The optimized structure of the non-activated C_2N (a), end-on adsorption of the N_2 molecule on the -CN group (b), side-on adsorption of N_2 molecule on the -CN group (c), and end-on adsorption of N_2 molecule on the pyrazinic nitrogen (d). The N_2 molecule has been marked with a brown circle.

Supplementary Tables

Table S1. C and N contents in HAT-Ts determined with EA, EDX, and XPS.

HAT-Ts	C (at%)			N (at%)		
	EA	EDX	XPS	EA	EDX	XPS
HAT-700	48.8	66.7	51.3	25.1	30.9	28.5
HAT-950	70.6	84.3	78.2	12.8	10.3	11.3

Table S2. EA results of HAT-700 and HAT-700-A.

	C (at%)	N (at%)	H (at%)
HAT-700	48.8	25.1	2.3
HAT-700-A	42.2	19.7	1.9

Table S3. Nitrogen etching content of HAT-700 summary with different methods.

	EA	XPS	UV-Vis
etched-N (at%)	5.4	6.6	4.9

References

[1] a) J. T. Rademacher, K. Kanakarajan, A. W. Czarnik, *Synthesis* **1994**, *4*, 378-380; b) B. Kurpil, A. Savateev, V. Papaefthimiou, S. Zafeiratos, T. Heil, S. Özenler, D. Dontsova, M. Antonietti, *Appl. Catal. B-Environ* **2017**, *217*, 622-628.

[2] R. Walczak, B. Kurpil, A. Savateev, T. Heil, J. Schmidt, Q. Qin, M. Antonietti, M. Oschatz, *Angew. Chem. Int. Ed.* **2018**, *57*, 10765-10770.

[3] a) G. W. Watt, J. D. Chrisp, *Anal. Chem.* **1952**, *24*, 2006-2008; b) L. Zhou, C. E. Boyd, *Aquaculture* **2016**, *450*, 187-193.

[4] Y. Wang, Y. Yu, R. Jia, C. Zhang, B. Zhang, *Natl. Sci. Rev.* **2019**, *6*, 730-738.

[5] Z. Y. Wu, M. Karamad, X. Yong, Q. Huang, D. A. Cullen, P. Zhu, C. Xia, Q. Xiao, M. Shakouri, F. Y. Chen, J. Y. T. Kim, Y. Xia, K. Heck, Y. Hu, M. S. Wong, Q. Li, I. Gates, S. Siahrostami, H. Wang, *Nat. Commun.* **2021**, *12*, 2870.

[6] a) G. Kresse, J. Furthmuller, *Comput. Mater. Sci.* **1996**, *6*, 15-50; b) G. Kresse, J. Furthmüller, *Phys. Rev. B* **1996**, *54*, 11169-11186.

[7] P. E. Blöchl, *Phys. Rev. B* **1994**, *50*, 17953-17979.

[8] J. P. Perdew, K. Burke, M. Ernzerhof, *Phys. Rev. Lett.* **1996**, *77*, 3865.

[9] S. Grimme, J. Antony, S. Ehrlich, H. Krieg, *J. Chem. Phys.* **2010**, *132*, 154104.

[10] J. K. Nørskov, T. Bligaard, A. Logadottir, J. R. Kitchin, J. G. Chen, S. Pandelov, U. Stimming, *J. Electrochem. Soc.* **2005**, *152*, J23.